SLAC–PUB–3938
April 1986
(E/I)

The Rotor Electrometer:
A New Instrument for Bulk Matter Quark Search Experiments*

JOHN C. PRICE[a], WALTER INNES, SPENCER KLEIN AND MARTIN PERL

Stanford Linear Accelerator Center
Stanford University, Stanford, California 94305

Abstract

The rotor electrometer is a new instrument which we hope will make possible searches for rare fractionally charged impurities in very large quantities of matter. The ultimate goal of the project is to be able to measure the net charge of 10 mg samples of any material to an accuracy of .05 q_e in a few minutes (q_e is the electron's charge). This paper reports the achievement of sub-electron (.3 q_e) charge resolution with the new device. We discuss effects which limit the resolution and consider prospects for improving the performance to the point where a fractional charge search may be attempted.

Submitted to Review of Scientific Instruments

---

* Work supported by the Department of Energy, contract DE-AC03-76SF00515.

[a] Present address: Department of Physics, Stanford University, Stanford, California 94305

Introduction

The strongly interacting elementary particles are described as bound states of constituents called "quarks", which carry fractional charge of $\pm 1/3$ or $\pm 2/3\, q_e$, where q_e is the charge of the electron. It was originally assumed that if quarks are the elementary constituents of hadrons, then objects with net fractional charge must exist. Today, because of the negative results of many searches for fractional charge[1] it is believed that quarks are "confined" inside hadrons. "Free quarks", and combinations of quarks with net fractional charge, are thought not to exist.

However, it may be that fractionally charged particles do exist but are very rare. In 1977, and again in 1979 and 1981, Fairbank, Hebard, LaRue, and Phillips reported observations of fractional charge on 100 μg niobium spheres[2]. This positive result, still unconfirmed, has stimulated a new generation of fractional charge search experiments[3]. Their goal is to search as large a quantity of material as possible, and to search many different substances. Present techniques are limited to at most a few milligrams, and usually to materials with special properties.

This paper describes a new charge measuring instrument, the rotor electrometer, that we have developed with the goal of pushing the search for fractional charge beyond the milligram level. We hope to be able to measure a 10 mg sample of any composition in a few minutes, so that as much as a gram of material could be searched in a day. The new instrument differs from others used previously in that it does not rely on the detection of a small force. Instead, a small alternating voltage is generated by rapidly varying the capacitance between a small conducting sample container and a high impedance amplifier. A high speed rotor with an active magnetic bearing is used to implement the varying capacitance. A somewhat similar device has recently been proposed by Williams and Gillies[4].

The rotor electrometer described here is the third in a series of similar instruments built by our group. The first two instruments achieved charge sensitivities of 100 q_e and 5 q_e respectively, and have been described briefly elsewhere[5]. The present instrument has a resolution of .3 q_e for measurements of changes in the charge of a

single sample. The calibration is obtained by observation of single electron changes in the sample charge. The sensitivity is presently limited by amplifier noise, sample motion, and an unidentified noise source.

Some improvement in the charge resolution must still be made before a fractional charge search can be attempted, and also the technique must be extended to absolute measurements of the sample charge, or at least to absolute measurements of the difference between the charge of two samples. As will be explained below, because the instrument is very sensitive to small motions of the sample (or sample container), extending the method to absolute charge measurements presents some difficulties, but may be possible with an improved device.

A more complete description of the rotor electrometer is available in the first author's thesis[6].

I. The Method

The basic principle, but not the actual geometry, of the rotor electrometer is illustrated in Fig. 1. A conducting sample with charge Q is moved periodically back and forth between two Faraday cups. The "signal cup" is connected to the input of a high impedance voltage measuring amplifier. When the sample is inside the signal cup a voltage Q/C appears at the amplifier input. The capacitance C is made as small as possible, limited by the amplifier's input capacitance. A second Faraday cup, the "ground cup", is required so that half a cycle later the sample charge will be shielded and the voltage at the amplifier input will drop to zero. The rms voltage generated per electron charge on the sample will be

$$v_e = \frac{1}{2\sqrt{2}} \frac{q_e}{C}.$$

Since the signal is periodic a lock-in amplifier can be used to limit the bandwidth through which noise may pass. If the total amplifier noise is represented as a voltage spectral density S_n (V^2/Hz) at the amplifier input then the rms fluctuations

due to the amplifier noise will be

$$v_n = \sqrt{\frac{S_n}{2T}},$$

so the resolution in units of the electron's charge is

$$\sigma_e = \frac{v_n}{v_e} = \frac{2C}{q_e}\sqrt{\frac{S_n}{T}},$$

where T is the time over which the lock-in's output is averaged. The parameters for the rotor electrometer are $C = 4.3\,\mathrm{pF}$ and $\sqrt{S_n} = 8.8\,\mathrm{nV}/\sqrt{\mathrm{Hz}}$ (at the 7.2 kHz signal frequency) which gives

$$\sigma_e = .47 \times \sqrt{\frac{1\,\mathrm{sec}}{T}}.$$

In practice the resolution is not this good. We lose a factor of three in signal due to electrostatic inefficiencies, the total noise is a factor of two above the amplifier noise, and also the averaging time is limited to $T = 200\,\mathrm{sec}$ by low frequency drifts.

II. Description of the Instrument

The mechanical arrangement of the actual device is shown in Fig. 2. Instead of moving the sample back and forth between the Faraday cups, the sample is held fixed and the cups are moved. In earlier devices the cups were three-sided, but in the present device they have been reduced to one-sided pads in order to reduce the stray capacitance from cup to cup. Eight signal pads and eight ground pads, each 2.5 mm wide and 5 mm high, are spaced around the perimeter of the high speed rotor. As the rotor spins, the sample charge is alternately coupled to the amplifier by a signal pad, and then shielded from the amplifier by a ground pad. Neglecting inefficiencies, a peak-to-peak voltage Q/C appears at the amplifier input, where Q is the sample charge, and $C = 4.3\,\mathrm{pF}$ is the total capacitance of the signal pads to ground, due in part to the total stray capacitance from each signal pad to the adjacent ground pads (2.8 pF), and in part to the amplifier input capacitance (1.5 pF).

The rotor is 18 cm long and 3 cm in diameter. It is made mainly of a single piece of polystyrene, chosen for its high stiffness, low dielectric constant, and small dielectric loss angle. The rotor spins in high vacuum on an active magnetic bearing at 900 Hz. The charge measuring signal is at $8 \times 900\,\mathrm{Hz} = 7.2\,\mathrm{kHz}$. A 4-inch oil diffusion pump with a liquid nitrogen cold trap keeps the chamber pressure below 10^{-6} torr. The drag on the rotor is such that the deceleration is only .3 Hz/hour when the drive motor is turned off. This allows data collection with the rotor coasting, so that noise generated by the motor is not a problem.

The ground pads are capacitively coupled to ground and the signal pads are capacitively coupled to the low noise amplifier. The ground pads and signal pads, the rotating halves of the signal and ground coupling capacitors, and the four reflective tachometer pads are all plated in copper onto the surface of the polystyrene rotor body. The signal coupling capacitor gap is 1.0 mm and the capacitance is 11.4 pF. The lower half of the signal coupling capacitor is made of copper-plated aluminum and is mounted on a quartz glass insulator. The 18.5 pF cylindrical ground coupling capacitor has a 2.2 mm gap and the outer half is also made of copper-plated aluminum. It is bolted to the ceiling of the vacuum chamber.

Figure 3 is a photograph of the signal generating part of the apparatus with a test sample installed. The n-channel JFET which forms the first stage of the low noise amplifier is visible below the signal coupling capacitor.

The sample is hung from a quartz glass fiber along the left edge of the rotor next to the pads. Figure 4 shows details of a typical sample used to study the instrument. The quartz glass fiber is chosen for its excellent insulating properties, and indium has been used for test samples because it sticks to the glass fiber. A thin strip of latex rubber damps the motions of the sample. The sample manipulator arm exits the chamber through a flexible bellows, and is attached to a precision manipulator outside the vacuum so that calibrated motions of the sample may be made. Crude adjustments of the sample charge are made with a fine wire probe which is connected to an adjustable potential. An ultraviolet light is used to make precise adjustments of the charge by photoemission.

The upper part of Fig. 2 shows the active magnetic bearing which allows the rotor to spin at high speeds with low vibration. Earlier versions of the instrument used ball bearings, but these were not satisfactory because of vibrations which generated microphonic signals, and because of electrical noise due to the metal-to-metal contacts in the bearings. The active magnetic bearing now employed is based on designs developed by J. W. Beams and co-workers[7].

A samarium cobalt permanent magnet generates a solenoidal magnetic field which supports the weight of the rotor. This arrangement is stable horizontally, so that the rotation axis is drawn to the magnetic axis, but the vertical equilibrium point where the upwards magnetic force equals the downwards force of gravity is unstable, so the vertical motions must be controlled by a servo system. The LED, lenses, and split photodiode are used together with the suspension electronics (see Fig. 5) to measure the vertical position of the rotor. The electronics supply a correction current to the servo coil, which generates a trim magnetic field that pushes on the rotor to make its vertical motions about the equilibrium position stable and damped.

To provide damping of the horizontal motions of the rotor, the permanent magnet is free to move horizontally in a viscous oil bath. The magnet is hung as a pendulum from a point 12 cm above the top of the rotor. This arrangement was not sufficient to damp the slow (6 second period) gravitational precession of the rotor, so an active horizontal damping circuit was added, as shown in Fig. 5. A separate lock-in amplifier demodulates the 900 Hz fundamental signal, which is sensitive to the horizontal position of the rotor. After spin-up, the (near dc) output of the damping lock-in is differentiated and applied to the rotor drive coils. The magnetic field generated by the coils applies a small torque to the magnetic moment of the rotor's ferromagnetic bearing. If the lock-in phase is set correctly, this torque can be used to damp the precession.

The rotor is driven by a simple reluctance motor. The ferromagnetic armature, made of alloy 4750 nickel iron, is shown in Fig. 2. The rotor drive coils (not shown

in Fig. 2) are mounted outside the glass tube which houses the upper part of the rotor. The two coils are each 70 turns of #18 Cu wire on 3 cm diameter forms. The rotor drive electronics (see Fig. 5) supplies an 8 A current at a 50% duty cycle to the drive coils, resulting in a peak torque of about 1400 dyne-cm and an average acceleration of about 1 Hz/sec, so that the rotor may be spun up to 900 Hz in 17 minutes. A reversing switch is included so that the rotor may be spun-down in the same amount of time.

Four reflective copper pads on the rotor are illuminated by an LED and viewed by a photodiode to provide a tachometer. The LED and photodiode are mounted on a ring concentric with the rotor axis that may be rotated to adjust the tachometer phase. The tachometer signal is required for the rotor drive and also as a phase reference for the two lock-in amplifiers in the system.

Figure 6 shows the low noise preamplifier circuit. Although the charge measuring signal is always at 7.2 kHz, the preamplifier is broadband (500 Hz – 20 kHz). This has been useful for diagnostic purposes, and because the 900 Hz signal is used for the horizontal damping. No gate bias resistor is needed at the preamplifier input. The JFET will automatically bias with the gate-source voltage near zero, which is its most quiet operating point.

Care has been taken in the preamplifier design to insure that there are no significant noise sources outside the first stage JFET. The total contribution of the power supplies, the following stages, and the first stage bias resistors is $.7\,\mathrm{nV}/\sqrt{\mathrm{Hz}}$ at 7.2 kHz when referred to the input.

With a 2.8 pF dummy load connected to the preamplifier to simulate the capacitance of the apparatus, the total noise referred to the preamplifier input is $8.8\,\mathrm{nV}/\sqrt{\mathrm{Hz}}$ at 7.2 kHz. The measured preamplifier input capacitance C_{in} is 1.5 pF. The 2N3686 first stage JFET was selected from 25 tested devices, of types 2N3686, 2N4416, 2N4117, and 2N4220. The device chosen had the smallest value of $C \cdot \sqrt{S_n}$, where C is the total capacitance, 2.8 pF + C_{in}, and $\sqrt{S_n}$ is the total noise referred to the input. The forward transconductance of the chosen device is 2 mS.

The signal processing chain which follows the preamplifier is shown in Fig. 5.

The typical signal amplitude at 7.2 kHz is 1 to 10 μV rms (referred to the preamplifier input), while the signal at 900 Hz is typically 100 times larger. Because of this a bandpass filter at 7.2 kHz is needed to remove the 900 Hz signal so that it will not saturate the lock-in input. The main lock-in amplifier[8] is followed by an anti-alias filter, an analog to digital converter, and the data logging computer. The computer is also interfaced to the ultraviolet light so that the data logging software can adjust the sample charge.

The instrument as described so far cannot be used for a fractional charge search, since an unknown background signal will be generated by charges on the quartz fiber, and also by other mechanisms. While the sensitivity to charges on the conducting sample may be directly measured (by ejecting photoelectrons, for example), charges on the fiber will be coupled to the instrument with an unknown efficiency and can mimic fractional charge.

Our proposed solution to this problem is shown in Fig. 7. A small conducting sample container is suspended by quartz fibers and the sample itself is placed deep inside the container. The charge is measured, then the sample is removed (perhaps by a small hook or tweezers), and the background signal generated by the sample container and fibers alone is measured. If the sample container is deep enough so that it forms a very good Faraday cup, then the sample-in signal minus the sample-out signal gives a measure of the net sample charge. One could alternatively replace the first sample with a second similar sample. Then the difference of the two readings would measure the difference of the net charges of the two samples, which is sufficient for a fractional charge search.

We have not yet tried to use a sample container in the instrument. So far we have only studied the noise and resolution of the instrument using samples like the one shown in Fig. 4.

III. Design Considerations

The basic features of the present design follow from the choice of sample size, together with the amplifier noise properties, and some aspects of the mechanics of

high speed rotors.

Since we wish to measure 10 mg samples, the sample dimensions must be about 1 mm × 1 mm × 1 mm. To provide good shielding, the sample container should be several times deeper than it is wide, for example a small can 1.5 mm in diameter and 4 mm high might be adequate. The pads should be about the same size as the sample container. If they were much smaller the coupling efficiency would suffer, while if they were much larger there would be unnecessary stray capacitance from pad to pad. Some preliminary electrostatics studies with a ×10 scale model have led us to the present dimensions. They are reasonable but perhaps not strictly optimal.

Once the pad geometry is chosen the rotor diameter follows from a choice of the number of pads, or equivalently the signal harmonic number. One pair of pads would seem to be the optimal choice from the point of view of stray capacitance. Unfortunately there is a very large signal generated at the fundamental (100 – 1000 μV rms, at the amplifier input), apparently due to the surface potentials in the coupling capacitor gaps. This signal changes by about 1 μV per 1 μm change in the rotor position, so that if the fundamental were also the signal frequency it would be necessary to hold the rotor fixed to about .25 nm during the measurement period. (The actual calibration of the instrument is 4.7 nV/q_e, so for a resolution of .05 q_e systematic effects must be held below .25 nV.) Instead we use the eighth harmonic for the signal frequency, where the background signal with no sample present is only 1 μV rms, and the signal only changes by .5 nV per 1 μm of motion of the rotor relative to the coupling capacitors. Thus the rotor must be held stationary only to .5 μm, which is required anyway because of the sensitivity to motions of the rotor relative to the sample.

The required signal frequency follows from the amplifier noise properties. Because of the high impedance of the capacitive signal source, the total noise rises very rapidly at low frequencies. The amplifier noise limited S/N doubles between 4 kHz and 8 kHz, but only increases by about a factor of 1.5 in going from 8 kHz to 16 kHz. While it is always better to spin faster, because of mechanical considerations to be discussed below, 7.2 kHz was used as the signal frequency.

Two difficulties arose in attempts to reach the required spin speed. First of all, it was found to be impossible to pass through flexural critical speeds. These are the rotation frequencies equal to the frequencies of the transverse flexural normal modes of the rotor. At these speeds prototype rotors deformed so much that they hit the sides of the vacuum chamber. Although many high speed ball bearing systems are able to pass quickly through shaft critical speeds without damage, it seems to be difficult to apply sufficient torque to a high compliance magnetic bearing system. The solution we have adopted is simply to make the rotor sub-critical. It has been possible to make the rotor stiff enough so that the first transverse flexural mode is at 1220 Hz, well above the 900 Hz spin speed. To obtain a high critical speed it is helpful to make the rotor hollow. The walls of the present design are 2.5 mm thick, except in the pad region where they are thinned to 1.2 mm to help reduce the stray capacitance from pad to pad.

The second major difficulty in reaching high speeds is an instability of the "forward whirl" which appears in this type of bearing. The basic mechanism was apparently first understood by MacHattie[9], and a detailed discussion is given in Ref. 6. The forward whirl is a gyrodynamic normal mode of the system, which at very high speeds is identical to the precession of a free symmetric top. The frequency of the whirl mode is proportional to the spin speed (for our rotor the whirl is at 42 Hz when the spin speed is 900 Hz), and because of the mass of the suspension magnet, the damping of the mode due to the oil bath decreases as the rotor spins faster. When there are magnetic losses in the bearing a force arises, increasing with the spin speed, which can drive the forward whirl. As the spin speed is increased eventually the driving force exceeds the damping, and the whirl mode becomes unstable.

Our first prototype of essentially the present design had a bearing made of 1018 cold rolled steel, and had a whirl instability threshold at 400 Hz. The next rotor had a bearing made of unannealed alloy 4750 nickel iron, a lower loss material. It began to whirl at 600 Hz. The present bearing is of annealed alloy 4750. The whirl threshold is now at 1000 Hz, allowing routine operation at 900 Hz with no

observable whirl.

IV. Performance

The instrument has so far been studied in three stages. First with no sample, then with a sample but without induced charge changes, and then finally with a sample and with periodic charge changes induced by photoemission.

With no sample the total noise observed is simply the $8.8\,\mathrm{nV}/\sqrt{\mathrm{Hz}}$ noise of the preamplifier, and the spectrum seen at the output of the lock-in amplifier is flat down to the lowest frequencies of interest (about 1 mHz). This measurement ensures that there is no extra noise contribution from the filters, the lock-in amplifier, the sampling, or the digitization.

When a sample is installed the instrument becomes very sensitive to small motions of the sample relative to the rotor. It thus becomes important to fully characterize the motions that are present in the system. By using the available information—the 7.2 kHz signal, the 900 Hz signal, and signals in the bearing servo electronics—it has been possible to obtain spectra of the motions in three orthogonal directions. The sensitivity to motions may be measured by using the sample manipulator to make calibrated translations of the sample. By combining the measured motion sensitivity of a given sample with the motion spectra, it has been possible to calculate the contributions that motions make to the total noise.

Many attempts were made to reduce the motion sensitivities of samples. Flowing ionized N_2 gas over the quartz fiber to discharge it was helpful, as were changes in the sample geometry. With a sample of the sort shown in Fig. 4, but without the guard, the best motion sensitivities achieved were about $20\,\mathrm{nV}/\mu\mathrm{m}$. The motion amplitudes are 1 to $2\,\mu\mathrm{m}/\sqrt{\mathrm{Hz}}$ at the important frequencies of a few mHz, so the motional noise was 20 to $40\,\mathrm{nV}/\sqrt{\mathrm{Hz}}$, well above the amplifier noise. The situation was finally improved by adding the guard. It is a small additional piece of indium, $.35\,\mathrm{mm} \times .35\,\mathrm{mm} \times .25\,\mathrm{mm}$, pinched onto the quartz fiber 4.3 mm above the sample, as shown in Fig. 4. The guard is placed well above the sample where the coupling to the pads is reduced, but where the coupling has a large dependence on the vertical

position. By carefully adjusting the charge of both the sample and the guard it is possible to nearly null the motion sensitivity in both the vertical and the radial directions. In the third direction the motions are small enough so that the total motional noise can be made less than or at least comparable to the amplifier noise. All of the data presented below was recorded with the most recent sample, which is the only guarded sample studied so far. The sample dimensions are as in Fig. 4, and the sample weighs 1 mg.

To make a measurement in a fractional charge search, one would first average the lock-in output for a time T, then change the contents of the sample container, and then average for a time T again. The difference of the two averages gives a measure of the sample charge. To simulate such a measurement we have made data runs where we average the output for a time T, then flash ultraviolet light on the sample to eject a few photoelectrons, and then average again for a time T. This is repeated many times, and the difference of consecutive averages is histogrammed. Peaks appear in the histogram where the sample charge has changed by one, two, or more electrons. The spacing of the peaks gives a calibration of the instrument, and the widths give a measure of the resolution. To more simply study the noise we have also taken data and generated histograms without flashing the ultraviolet light between averaging periods.

Figure 8 shows two typical histograms obtained without flashing the light. Each contains about seven hours of data. The averaging time was 200 seconds, which is the longest time that can be profitably used because the noise spectrum rises rapidly at low frequencies. It has been necessary to subtract a linear fit from each data run because of a nearly linear drift in the data. The drift rate varies from run to run, and is usually about 1 nV/200 sec, but was as high as 37 nV/200 sec in one run. The slope of the fit is set equal to the average of the slopes of the 200 second segments. This information will still be available when there are unknown changes in the signal between each 200 second period.

Figure 9 shows the measured rms widths of all the runs made without flashing the light. The squares give the observed widths, while the diamonds give the

contribution to the widths which can be accounted for by the sum of the amplifier noise and the motional noise. The dotted line gives the amplifier noise contribution alone:

$$v_n = \frac{\sqrt{2} \cdot 8.8\,\mathrm{nV}/\sqrt{\mathrm{Hz}}}{\sqrt{2 \cdot 200\,\mathrm{sec}}} = .62\,\mathrm{nV}.$$

The factor of $\sqrt{2}$ in the numerator of this expression occurs because there are two averaging periods contributing to each data point in the histograms. The motional contribution is different for each run because of differences in the sample motion sensitivity. The motional noise contribution is always smaller than the amplifier noise contribution.

There is an important contribution to the total noise that remains unexplained. The average unexplained contribution to the total widths is 1.2 nV, unchanging from run to run within the statistical uncertainties. Figure 10 shows a spectrum of the total noise for runs 3 and 4. The unexplained contribution is dominant in both spectra below about 3 mHz, and it rises rapidly at lower frequencies. The unexplained noise may be due in part to spontaneous charge changes caused by cosmic rays or radioactivity, but a search for steps in the data shows that less than half of the extra noise can be accounted for in this way. We hope that future tests with different samples will provide a clue as to the source of the unexplained noise.

Figure 11 shows histograms for data runs in which the light was flashed between the averaging periods. The light intensity was changed from run to run, but kept constant during any one run. Run 12 seems to be somewhat noisier than the others. It may be that a piece of dust was transferred to the sample when it was reneutralized part way through the run.

In run 13 peaks due to the emission of one, two, three, and four photoelectrons are visible. The peaks are spaced by 4.7 nV, so the instrument's calibration is $4.7\,\mathrm{nV}/q_e$. Since (from the data in Fig. 9) the mean observed noise is 1.5 nV, the measured resolution is $.3q_e$.

From the measured total capacitance of 4.3 pF one should actually expect the calibration to be $13\,\mathrm{nV}/q_e$. Since it is only $4.7\,\mathrm{nV}/q_e$, the instrument is inefficient

by a factor of 2.8. Some of the inefficiency is due to the finite size of the coupling capacitances and to imperfect sample to pad coupling.

V. Prospects for a Fractional Charge Search

Before a fractional charge search can be attempted we must first improve the resolution (as measured above) by a factor of six to reach $.05\,q_e$, and then must extend the technique to absolute charge measurement.

To improve the resolution we must reduce the unexplained part of the noise, the motional noise contribution, and the amplifier noise contribution. The unexplained noise must be reduced by a factor of five. We don't know if this can be done, but several tests could be made to help us understand the problem. In particular we would like to see how changes in the fiber diameter and sample size effect the unexplained noise.

The motional noise usually contributes about $.15\,q_e$ to the resolution, so it must be reduced by a factor of three. This could be done either by reducing the motion sensitivities, or by reducing the motions themselves. The motion sensitivities could be reduced by the addition of a second guard or perhaps by changes in the pad geometry. With a properly placed second guard one could null the motion sensitivity in all three directions, because one would have the charge of three objects available for adjustment. The motions could be reduced by improving the magnetic suspension electronics and by using low thermal expansion materials, or by more careful temperature control.

The amplifier noise contribution also must be reduced by a factor of three. Improvements could be made by cooling the JFET[10], by increasing the spin speed, by improving the electrostatic efficiency, or by increasing the averaging time. Some combination of these steps will probably be necessary.

If it should prove difficult to decrease each of the noise contributions then one could still improve the resolution by making multiple measurements of the same sample.

Once the resolution is improved we must then install a sample container in the

instrument so that absolute charge measurements can be made. The difficulty here is that the sample container position must not be changed when the sample is changed. Since the best motion sensitivities achieved so far are $1\,\mathrm{nV}/\mu\mathrm{m} = .2\,q_e/\mu\mathrm{m}$, we must maintain the sample container's position to about 250 nm to keep the systematic effects below $.05\,q_e$. It will certainly be helpful to swap two identical samples, rather than to go from a full sample container to an empty one, in order to keep the weight constant.

The 250 nm requirement could be relaxed if the motion sensitivity could be reduced, perhaps by the addition of a second guard. Unfortunately it will still be necessary to keep the relative sample to guard positions fixed to high accuracy. In an improved device it would seem very worthwhile to have some way of constantly monitoring the important motions.

VI. Summary

The rotor electrometer is a new electronic instrument for fractional charge search experiments. A high speed rotor with an active magnetic bearing is used to rapidly vary the capacitance between a conducting sample and a high impedance preamplifier. In principle a resolution of $.05\,q_e$ may be obtained in a few minutes.

The instrument has so far reached a resolution of $.3\,q_e$ for measurements of changes in the sample charge. The resolution is limited by amplifier noise, sensitivity to motions, and an unexplained effect. Besides the need to improve the resolution, a major outstanding problem is to extend the method to absolute charge measurement. This is made difficult by the instrument's sensitivity to motions of the sample container relative to the rotor.

Acknowledgments

The authors would like to thank Ronald Baggs, Kenneth Hughes, Robert Leonard, Thomas Nakashima, and Ronald Stickley for their assistance.

REFERENCES

1. L. W. Jones, Rev. Mod. Phys. **49**, 717 (1977); L. Lyons, Progress in Particle and Nuclear Physics **7**, 157 (1981); G. Susinno, in *Proc. of the Int. Conf. on Physics in Collision: High Energy ee/ep/pp Interactions, Blacksburg, Virginia, 1981*, Vol. I, edited by W. P. Trower and G. P. Bellini (New York, Plenum Press, 1982) p.33.
2. G. S. LaRue, W. M. Fairbank, and A. F. Hebard, Phys. Rev. Lett. **38**, 1011 (1977); G. S. LaRue, W. M. Fairbank, and J. D. Phillips, Phys. Rev. Lett. **42**, 142 (1979); G. S. LaRue, J. D. Phillips, and W. M. Fairbank, Phys. Rev. Lett. **46**, 967 (1981).
3. D. Joyce *et al.*, Phys. Rev. Lett. **51**, 731 (1983); M. A. Lindgren *et al.*, Phys. Rev. Lett. **51**, 1621 (1983) and references therein; R. G. Milner, B. H. Cooper, K. H. Chang, K. Wilson, J. Labrenz, and R. D. McKeown, Phys. Rev. Lett. **54**, 1472 (1985); P. F. Smith, G. J. Homer, J. .D. Lewin, H. E. Walford, and W. G. Jones, Phys. Lett. **153B**, 188 (1985); G. Hirsch, R. Hagstrom, and C. Hendriks, Lawrence Berkeley Laboratory preprint LBL-9350 (1979).
4. E. R. Williams and G. T. Gillies, Lett. Nuovo Cimento **37**, 520 (1983).
5. W. Innes, S. Klein, M. Perl, and J. C. Price, preprint SLAC-PUB-2938 (1982).
6. J. C. Price, The Rotor Electrometer: A New Instrument for Fractional Charge Searches, Ph.D. thesis, Stanford University, 1985 (printed as SLAC-Report-288, Stanford Linear Accelerator Center, 1985).
7. J. W. Beams, J. D. Ross, J. F. Dillon, Rev. Sci. Instrum. **22**, 77 (1951). Many references to Beams' work are given by P. J. Geary, *Magnetic and Electric Suspensions,* (British Scientific Instrument Research Association, Kent, 1964).
8. Princeton Applied Research model #5402.
9. L. E. MacHattie, Rev. Sci. Instrum. **12**, 429 (1941).

10. F. Bordoni, G. Maggi, A. Ottaviano, and G. V. Pallottino, Rev. Sci. Instrum. **52**, 1079 (1981); S. Klein, W. Innes, and J. C. Price, Rev. Sci. Instrum. **56**, 1941 (1985).

FIGURE CAPTIONS

1. Principle of the rotor electrometer. Q is the sample charge and C is the total capacitance to ground.
2. Cut-away view of the instrument.
3. Signal generating part of the device. The front cover of the vacuum chamber has been removed for this photograph.
4. Test sample and sample mount. The sample is a small piece of indium foil pinched onto a quartz glass fiber. The guard reduces the instrument's sensitivity to motions (see section IV).
5. Block diagram. The signal lock-in is set to lock at twice the reference signal frequency. The reference signal is bandpass filtered to reduce phase noise.
6. Preamplifier schematic.
7. Use of sample container for background subtraction.
8. Histograms of the differences between consecutive 200 second averages of the output. In an actual measurement the sample would be changed between averaging periods. The calibration is $1q_e = 4.7\,\mathrm{nV}$.
9. The observed noises (solid) are the rms widths of histograms like those in Fig. 8. The explained noises (open) are the sum of the amplifier noise contributions and the motional noise contributions. The dotted line shows the amplifier noise level.
10. Spectra of the total noise referred to the input.
11. Histograms with charge changes. These histograms were generated in the same way as those in Fig. 8, except that the sample was exposed to a burst of ultraviolet light between each averaging period.

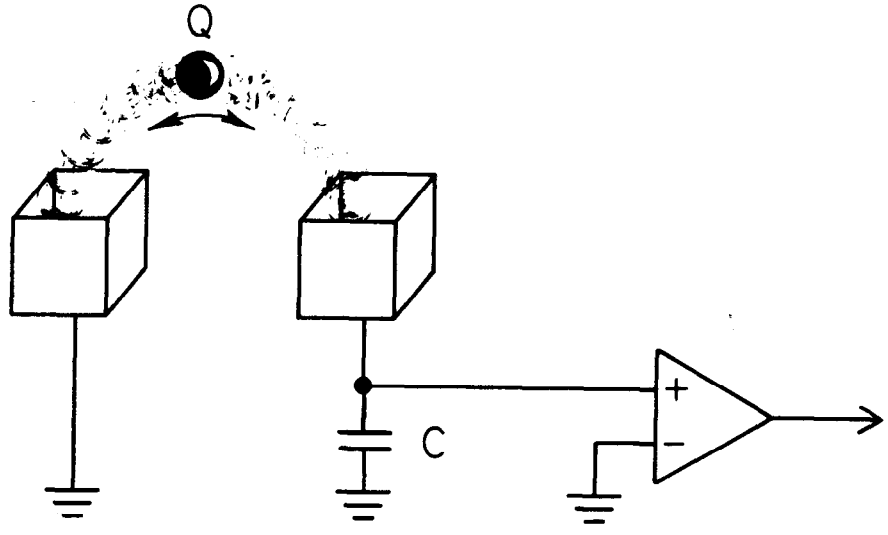

4-86

5393A1

Fig. 1

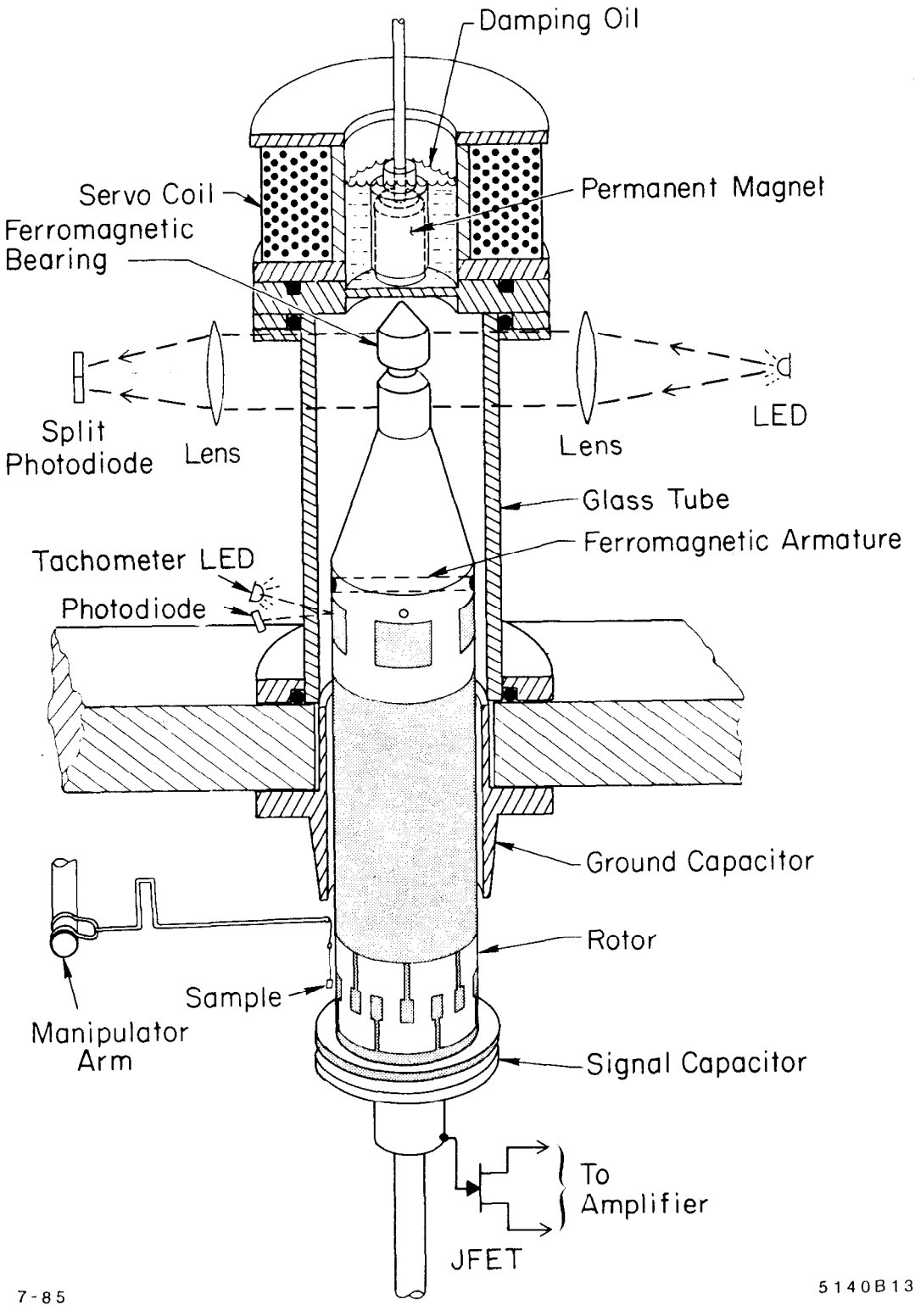
Damping Oil
Servo Coil
Ferromagnetic
Bearing
Permanent Magnet
Split
Photodiode
Lens
Lens
LED
Glass Tube
Ferromagnetic Armature
Tachometer LED
Photodiode
Ground Capacitor
Rotor
Sample
Manipulator
Arm
Signal Capacitor
To
Amplifier
JFET
7-85
5140B13

Fig. 2

Fig. 3

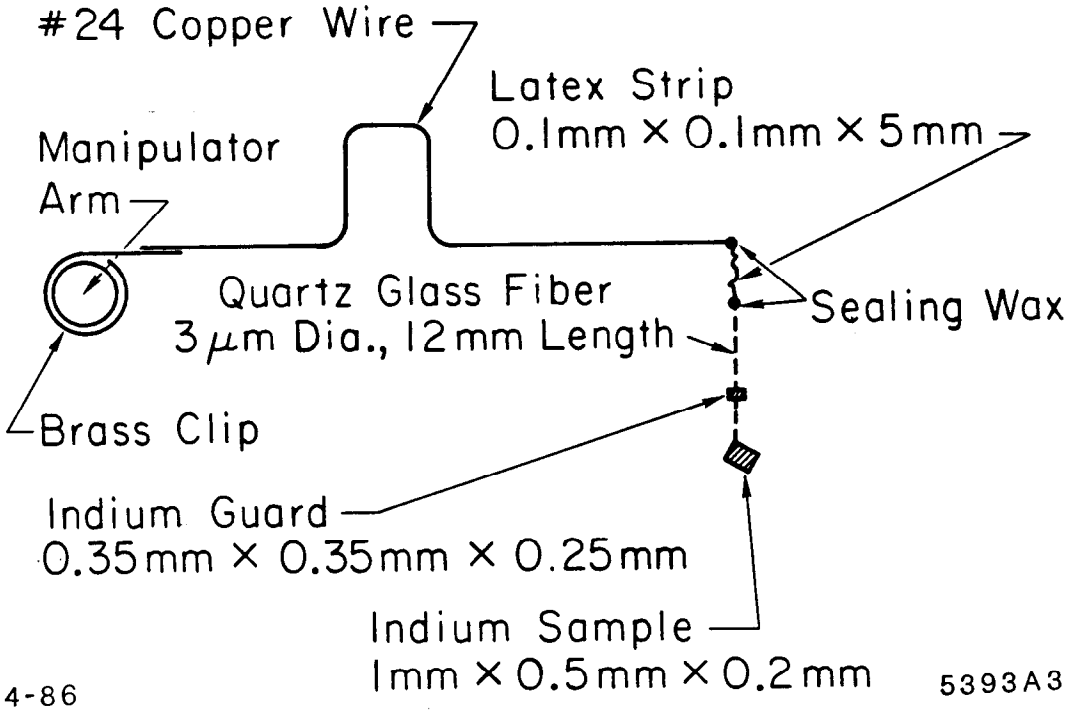
#24 Copper Wire
Latex Strip
0.1mm × 0.1mm × 5mm
Manipulator
Arm
Quartz Glass Fiber
3 μm Dia., 12mm Length
Sealing Wax
Brass Clip
Indium Guard
0.35mm × 0.35mm × 0.25mm
Indium Sample
1mm × 0.5mm × 0.2mm
4-86
5393A3

Fig. 4

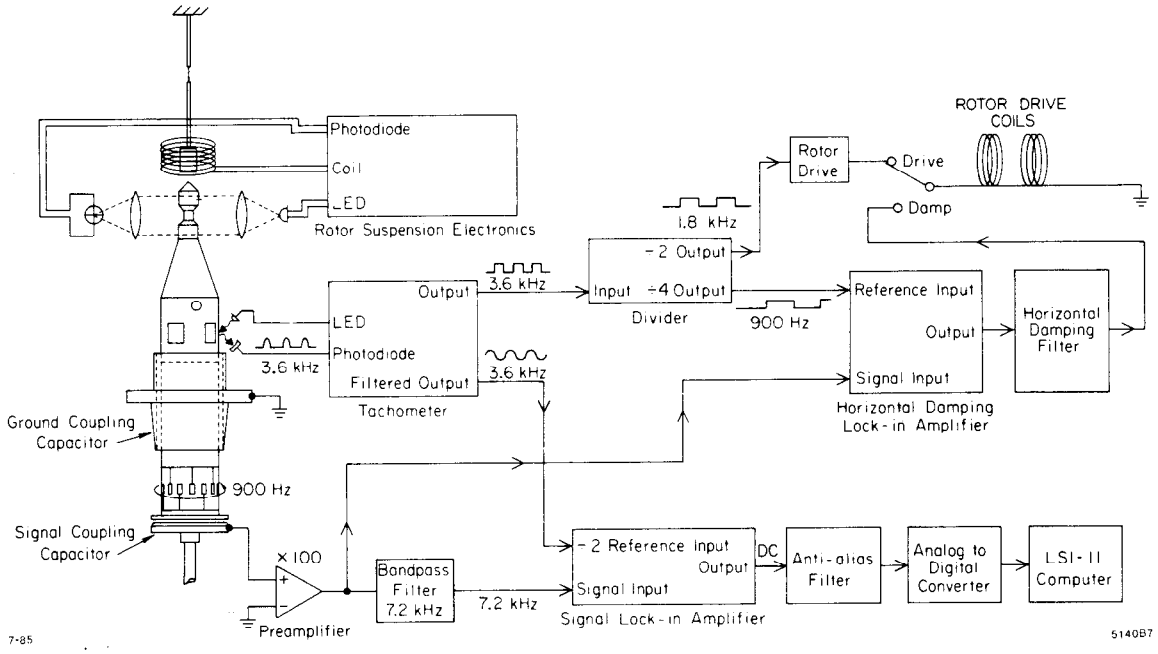
Photodiode
Coil
LED
Rotor Suspension Electronics
ROTOR DRIVE COILS
Rotor Drive
Drive
Damp
1.8 kHz
÷2 Output
Input ÷4 Output
Divider
900 Hz
Reference Input
Output
Signal Input
Horizontal Damping Lock-in Amplifier
Horizontal Damping Filter
Output
3.6 kHz
LED
Photodiode
Filtered Output
Tachometer
3.6 kHz
3.6 kHz
Ground Coupling Capacitor
900 Hz
Signal Coupling Capacitor
×100
+
-
Preamplifier
Bandpass Filter 7.2 kHz
7.2 kHz
÷2 Reference Input
Output
Signal Input
Signal Lock-in Amplifier
DC
Anti-alias Filter
Analog to Digital Converter
LSI-11 Computer
7-85
5140B7

Fig. 5

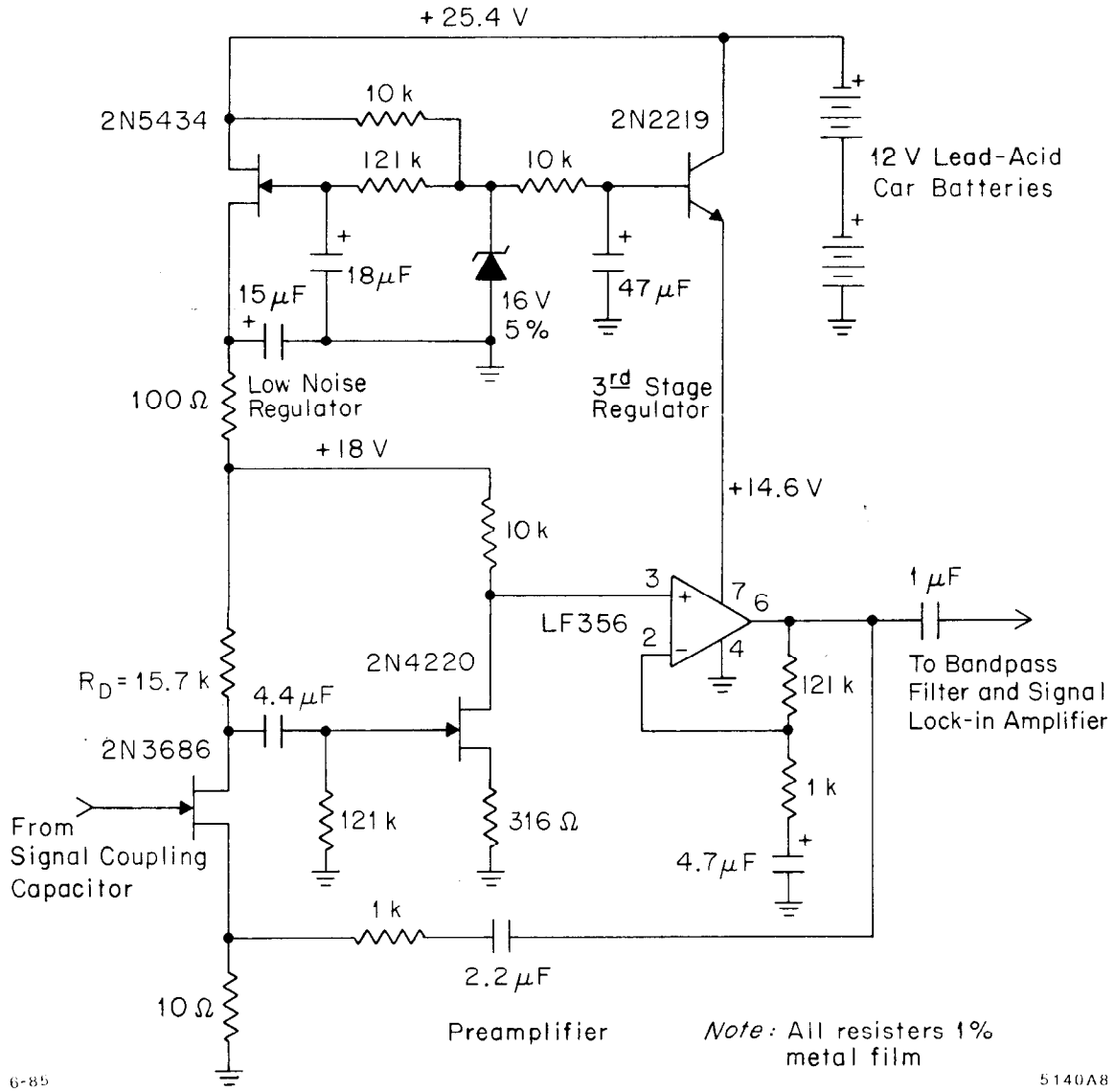
+25.4 V
10 k
2N5434
2N2219
121 k
10 k
12 V Lead-Acid
Car Batteries
18 μF
15 μF
16 V
5%
47 μF
100 Ω
Low Noise
Regulator
3rd Stage
Regulator
+18 V
+14.6 V
10 k
3
7
6
1 μF
LF356
2
4
2N4220
To Bandpass
Filter and Signal
Lock-in Amplifier
RD = 15.7 k
4.4 μF
121 k
2N3686
1 k
From
Signal Coupling
Capacitor
121 k
316 Ω
4.7 μF
1 k
2.2 μF
10 Ω
Preamplifier
Note: All resisters 1%
metal film
6-85
5140A8

Fig. 6

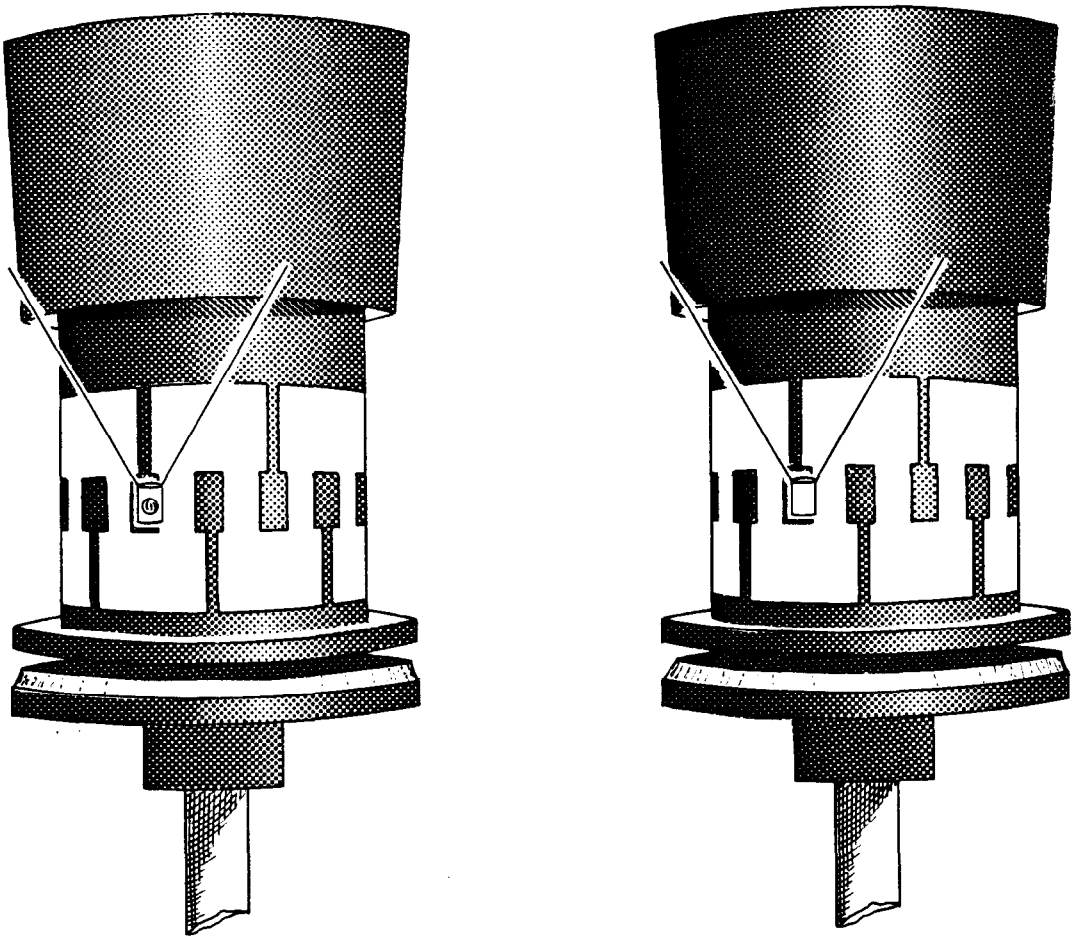

SAMPLE IN MINUS SAMPLE OUT

5-85

5140A2

Fig. 7

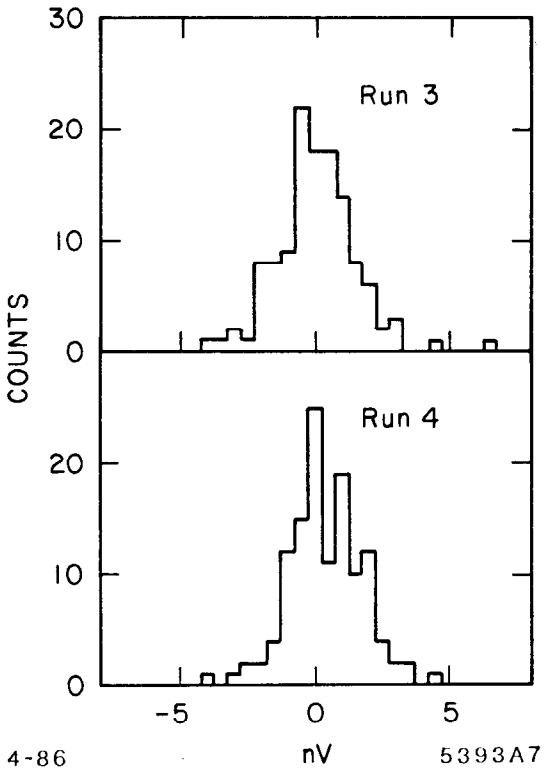

Fig. 8

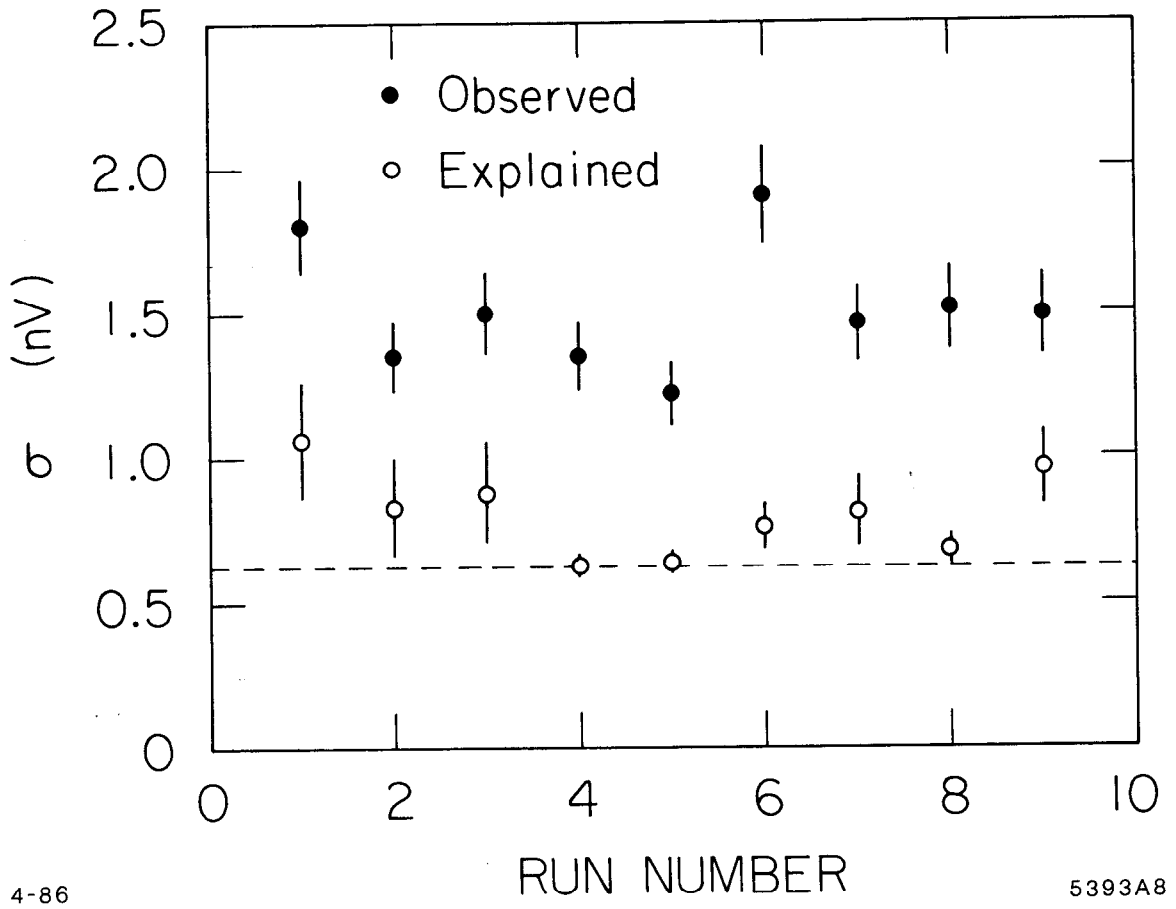
2.5
2.0
1.5
1.0
0.5
0
b (nV)
Observed
Explained
0
2
4
6
8
10
RUN NUMBER
4-86
5393A8

Fig. 9

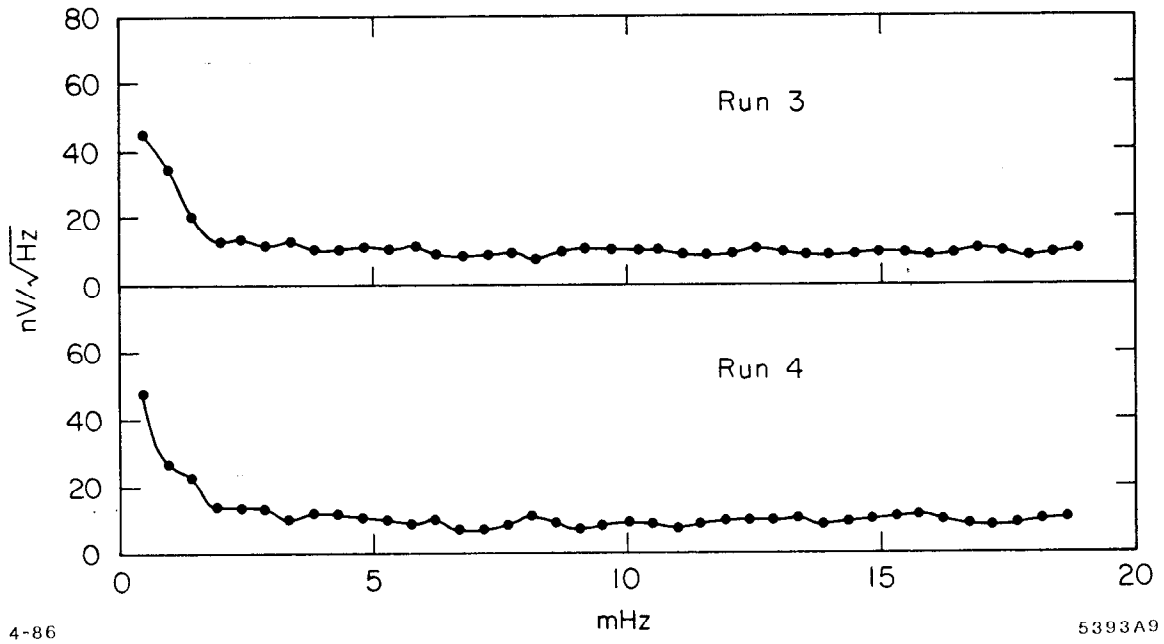

Fig. 10

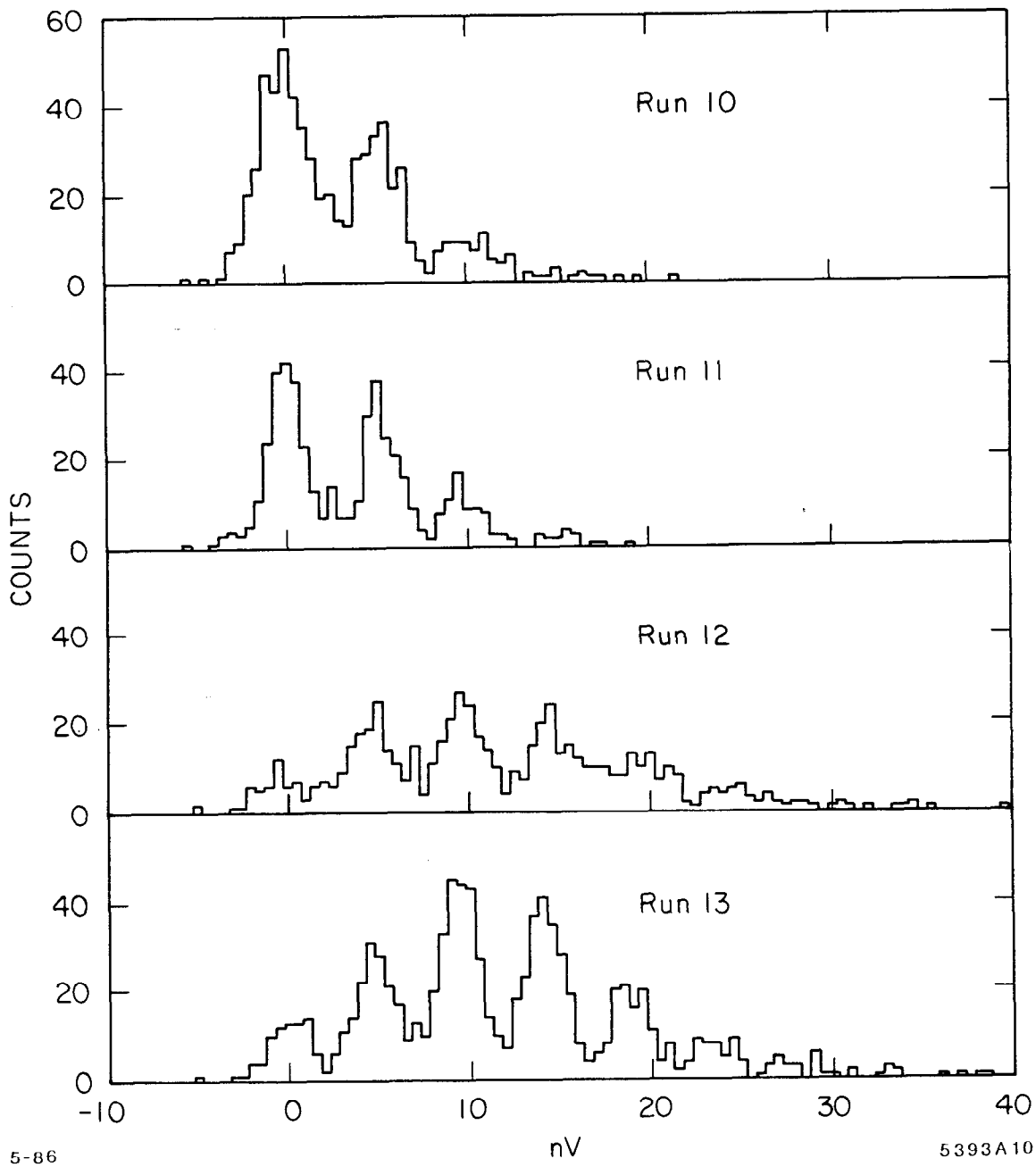

Fig. 11